Mechanical Systems and Signal Processing 191 (2023) 110126

Contents lists available at ScienceDirect

Mechanical Systems and Signal Processing

journal homepage: www.elsevier.com/locate/ymssp

# Damage identification during an impact event using the Hilbert-Huang transform of decomposed propagation modes

Stefano Cuomo [a], Marco Boccaccio [a], Michele Meo [b,*]

[a] Department of Mechanical Engineering, University of Bath, Bath BA2 7AY, UK
[b] School of Engineering, University of Southampton, Southampton SO17 1BJ, United Kingdom

ARTICLE INFO

Communicated by: Marc Rebillat

ABSTRACT

This work proposes a novel baseline-free method for real-time structural damage diagnosis during low-and high-velocity impact, based on the decomposition of the propagating modes caused by impact events. The high-frequency components (extensional) and the medium–low frequency components (flexural) of the measured waves are separated via Hilbert-Huang transform (HHT) through the intrinsic mode function (IMF), to obtain the amplitude and phase of the two extensional and flexural propagation modes. The Energy Ratio Ξ defined as the ratio between the maximum instant energy of the extensional mode and the maximum instant energy of the flexural mode is proposed. Results show that values of Ξ between 0 and 1 are a sign of low probability of damage during impact. When the Ξ parameter is reaching values higher than 1, penetration and perforation of the structure is likely to occur, since the extensional component in this scenario is more dominant than the flexural one. Tests were conducted on aluminium and CFRP samples with simple and complex geometries, subjected to low- and high-velocity impacts (with and without perforation) to validate the flexibility of the proposed method. Experimental results have demonstrated the effectiveness of the technique to discern elastic and damaging impact on different sample geometries and at different impact velocities in real-time and without the requirement of baseline datasets.

## 1. Introduction

Structural Health Monitoring (SHM) was introduced in aerospace industry decades ago as a high priority activity to assess the integrity state of structures, and nowadays it is widely applied in other fields such as automotive, marine, railways and medical. SHM is defined by the standard as the process of acquiring and analysing data from on-board sensors to evaluate the health of a structure [1]. The inspection activities are informed by the analysis from the monitoring process, leading to reduced maintenance costs and time, reduced downtime hence increased aircraft availability. These improvements can lead to the maintenance process approach from scheduled-based to condition-based increasing system reliability, as part of the prognostic health management of the structure [2,3]. The necessity to provide a continuous assessment of the structure's integrity rises from the tendency of aircraft or spacecraft to be exposed during life cycle to random impulsive loads such as impacts. Airborne debris during take-off or landing, bird strike during flight, space debris, ice, tool drop in maintenance operations, are all common cause of damage. In metallic material damage is generated as cracks that propagate under cyclic load. Composite materials are characterised by outstanding in-plane properties, light

* Corresponding author.
*E-mail address:* m.meo@soton.ac.uk (M. Meo).

https://doi.org/10.1016/j.ymssp.2023.110126
Received 6 September 2022; Received in revised form 6 January 2023; Accepted 9 January 2023
Available online 15 February 2023

weight, and high flexibility in manufacturing, but at the same time they are affected by low out-of-plane properties, making them susceptible to damage from any external impulsive load, such as the afore-mentioned impact types. In this class of material damage is generated as fibre breakage, matrix cracks and delamination. In some cases, out of plane loads induce a damage that is barely visible (BVID – Barely Visible Damage) and can grow until critical dimension with no evident signs on the external layers of the structure [4–6], leading to catastrophic failures. It is evident that the development of tools and techniques able to verify the state of structures plays a prominent role in the SHM analysis. In the last decades, different techniques have been proposed, i.e., ultrasound-guided waves [7–11], thermography [12,13], eddy current testing [14–17], vibration and modal analysis [18–22], computed tomography [23–27]. Acoustic emission (AE) has also been used for damage detection, localisation, and assessment. By definition, acoustic stress waves are perturbations that propagate through the structure generated by an impact or a localised load redistribution [28]. When an impact event occurs, transient elastic acoustic waves are induced through the material due to the redistribution of the stress field caused by the impact [29]. The way waves propagating in solids is described by different modes such as pressure waves, shear waves, flexural waves, Lamb and Rayleigh waves. These different types describe the particle motion, which in turn defines the wave propagation, e.g., in longitudinal waves, the motion is parallel to the wave direction, in shear waves the motion is perpendicular than propagation. Within the SHM context, guided waves (GW) have had great interest from researchers for damage assessment applications [30,31]. GW are mainly divided into shear (horizontal and vertical), Lamb and Rayleigh waves, and in each of them the propagation is limited through structures with well-defined boundaries [11,28,32]. Lamb waves (LW) defined as disturbances propagating within two parallel free surfaces have also gained research interests for SHM applications [33]. LW propagation typically occurs in plate-like structures, hence with thickness considerably smaller than the in-plane dimensions, and the wave propagation can be described by classical plate theory. When the wavelength is much larger than the plate thickness, two main Lamb wave modes are excited: extensional (symmetric) and flexural (antisymmetric) [34]. The former is dispersion less at low frequencies, whereas the latter is dispersive, i.e., its propagation velocity depends on the square root of the frequency [35]. AE methods developed on Lamb waves are extensively studied in literature as the thin plate hypothesis is occurring frequently in many common applications.

A novel baseline-free damage assessment method is proposed in this work, based on the decomposition of Lamb wave propagation modes via Hilbert-Huang transform. The HHT is the selected method, among other techniques, to separate the low frequency components from the high frequency ones because has been demonstrated to be the most effective tool to analyse non-linear and non-stationary data, as extensively discussed in the next section. The HHT, as mentioned before, was introduced as a data analysis tool for non-linear and non-stationary signals [36]. In [37] a damage metric is introduced using HHT to evaluate the state of curved composite panel with a pitch-catch method, proving to be a confident technique for tracking damage. In [38] the HHT is used as denoising filter and mode discrimination to separate propagating stress waves in concrete structure under compression and shear test. HHT proved to be an effective tool to separate overlapped lamb waves in aluminium plate and detect different modes [39]. In [40] the HHT is applied to extract instantaneous characteristics of guided ultrasonic waves to execute damage monitoring of a repaired aluminium panel and assess the curing level of symmetric composite laminates. In [41] this method was applied to assess the condition of utility timber poles, meanwhile in [42] exploited this tool to verify the rubbing fault of a rotary system. In this work, the HHT is used to extract characteristic features of signals from impact events to evaluate whether damage was induced after the strike. The rationale behind this research relies on a lack in literature to apply the HHT method to decompose transient signals generated by impact events. Indeed, here a novel damage parameter is introduced to qualitatively determine whether the impact caused indentation, penetration or perforation of the structure, without the necessity of a baseline, exploiting the proved ability of the HHT to decompose signals and discriminate modes. Furthermore, most of the techniques are based on active guided waves, while this paper exploits passive acoustic emission (AE) directly from impacts, from low to high velocity impact range. This method can assess in real-time if a structure is affected by serious detriment or critical damage caused by an impact event that could impair the global resistance and safety.

## 2. Hilbert-Huang transform

Signal analysis is the process of characterisation and study the basic properties of a specific set of data in the form of signals (e.g., electric field, sound waves, etc.). A signal is a function of many variables, but generally is the time and frequency dependency that is of particular interest to characterise a phenomenon [43]. The theory of frequency representation was introduced and developed by Fourier, with a common and effective signal processing tool as the Fourier transform. This technique anyway transforms data from time to the frequency domain, resulting in complete loss of time information and is valid as long as linearity and temporal stationarity (frequency not changing with time) are considered. Conventional methods for data-analysis rely on assumptions of linearity and stationarity. Methods for non-stationary data analysis, but only valid for linear time series, are spectrogram [44], Wavelet analysis [45,46], Wigner-Ville distribution [47], Evolutionary Spectral Analysis [48], Empirical Orthogonal Function [49]. Other techniques considered non-linear time series but stationary and deterministic systems. Real life systems are usually well described by non-linear and non-stationary assumptions; hence, any other hypothesis would diverge the description of the phenomenon from being physically meaningful. A typical characteristic of these type of phenomenon is their intra-wave frequency modulation i.e., instantaneous frequency variation within one period oscillation. To represent nonlinear and nonstationary data, it is necessary to have an adaptive basis. Adaptivity means that the definition of the basis function must be data dependent, i.e., a *posteriori*-defined basis, meanwhile the common mathematical approach for data analysis relies on *priori-defined functions*. The need to properly describe non-linear distorted waves affected by variations typically of non-stationary processes, motivated the development of innovative methods such as the Hilbert Huang transform (HHT)[50]. HHT is a data-analysis methodology exploiting an empirical approach, that is adaptive hence suitable for non-stationary and non-linear signals. Previous data analysis methods e.g., Fourier Transform mentioned before, were based on the imposition of linear structure on a nonlinear system, generating so-called harmonic distortions. The latter is the outcome

of using harmonics to depict the intra-frequency variation of nonlinear phenomena. They are mathematically correct but not physically meaningful [51]. To describe a non-linear and non-stationary system, the only physically consistent way is in terms of instantaneous frequency that can represent the continuous modulation of the wave frequency.

### 2.1. Hilbert Huang transform and IMF

The proposed method relies on the Empirical Mode Decomposition (EMD) by which any type of complex data can be decomposed into a finite small number of intrinsic mode functions (IMF) [36]. An IMF is defined as any function having the same number of zero crossing and extrema, and having symmetric envelopes defined by the local maxima and minima, respectively. The final output of the HHT represents an instant energy-instant frequency-time distribution of the considered dataset. The Hilbert transform is applied on the extracted IMF to retrieve instant frequency and energy components. Thus, for any real valued function $x(t)$ of $L^p$ class, the complex conjugate $y(t)$ is determined through the HT [50] by the following:

$$\mathscr{H}[x(t)] = \frac{P}{\pi}\int_{-\infty}^{+\infty}\frac{x(\tau)}{t-\tau}d\tau \tag{1}$$

where $P$ denotes the Cauchy principal value. The analytical signal $z(t)$ is given then combining the complex conjugate pair $x(t)$ and $y(t)$, thus:

$$z(t) = x(t) + iy(t) = a(t)e^{i\theta(t)} \tag{2}$$

where $\mathrm{a(t)} = \sqrt{[\mathrm{x^2(t)} + \mathrm{y^2(t)}]}$ represents the instantaneous amplitude and $\theta(\mathrm{t}) = \arctan[\,\mathrm{y(t)/x(t)}\,]$ is the phase function. The instantaneous frequency is derived by the following:

$$\omega = \frac{d\theta}{dt} \tag{3}$$

The instantaneous energy is simply derived by the amplitude, by the following:

$$E_i = |a_i(t)|^2 \tag{4}$$

Eq. 1 is mathematically equivalent to the convolution of $x(t)$ with $1/t$, thus the local properties of the considered function or signal are highlighted.

For any function, the definition of instantaneous frequency has some restrictions to be physically meaningful, since the real part of the Fourier transform must only have positive frequency [36]. However, for signal processing, this global condition should be reflected in local restrictions, thus the function considered must be symmetric locally, with respect to the zero mean level and have the same number of zero crossing and extrema. Consequently, the signal considered must be mono component, i.e., there is a single frequency value representing one component at any given time. However, since real signals have, multiple instantaneous frequencies, the Empirical Mode Decomposition can be introduced to convert complex multi-component signal into Intrinsic Mode functions (IMFs), having a mono-component character whose instantaneous frequency hence is well defined [36]. The resulting IMFs represents the oscillation modes embedded in the signal, and respects two conditions: the number of extrema corresponds to the number of zero crossing (or differ at most by one); the mean value of the envelope defined by the local maxima and the envelope defined by the local minima is zero.

Each intrinsic mode obtained represents a simple oscillation, and at any given time, different modes of oscillation are superimposed to each other, composing to the whole complex signal. A single IMF is characterised by variable amplitude and frequency, in opposite to harmonic components. Once the dataset is decomposed into multiple IMFs via EMD, the instantaneous frequency can be obtained by applying the Hilbert transform to each mode function [50].

The core part of the decomposition method relies on the identification of the intrinsic modes, and the relative time scales. The latter is strictly related to the kind of process analysed and its energy distribution as a function of time and frequency. The method assumes that the intrinsic time scale is defined by the time interval between successive extrema, leading to improving the resolution of the oscillatory modes and applicable to non-zero mean data [36]. This local time scale definition ensures a good representation of the process and its intrinsic modes.

The decomposition process firstly identifies the local extrema of the considered signal. Then, all the maxima and minima are connected with a cubic spline, respectively, that ensure data continuity, derivative and curvature, generating an upper and a lower envelope covering all the data. The mean value of $m_1(t)$ of the two envelopes is calculated and then the difference between the signal $x(t)$ and $m_1(t)$ is the first component of the sifting process:

$$x(t) - m_1(t) = h_1 \tag{5}$$

where $h_1$ theoretically represent an IMF but can be a distorted one due to overshoots and undershoots, leading to new extrema or move or scale of the existing function. The sifting process is performed to cancel riding waves and produce a more symmetric wave profile, thus requiring several iterations. Hence, the obtained $h_1(t)$ is converted as the data to be sifted again, and the extrema are connected with a cubic spline, then the mean is constructed and finally the difference is calculated, as follows:

$$h_1 - m_{11} = h_{11} \tag{6}$$

These iterations are repeated as many times as needed to obtain an IMF, as follow:

$$h_{1(k-1)} - m_{1k} = h_{1k} \tag{7}$$

If $h_{ik}$ is an IMF, then is designed as:

$$c_1 = h_{1k} \tag{8}$$

In this new dataset $c_1$, there are still modes, with longer periods, to be extracted. Hence, removing the intrinsic mode evaluated from the original signal, we have a new dataset to apply the sifting process to:

$$x(t) - c_1 = r_1 \tag{9}$$

The quantity $r_1$ is called residual of the signal. This process is repeated to all the IMF extracted, until the final residual, $r_n$.

$$r1 - c_2 = r_2$$

$$r_{n-1} - c_n = r_n \tag{10}$$

With the sum of the IMFs evaluated and the final residual $r_n$, the original signal is given as follow:

$$x(t) = \sum_{i=1}^{n} c_i(t) + r_n(t) \tag{11}$$

Huang et Al. [36] also suggested a specific criterion by which the sifting process is stopped. This threshold is set by the evaluation of the standard deviation of two consecutive sifting outputs:

$$SD = \sum_{t=0}^{T} \left[ \frac{\left| h_{1(k-1)}(t) - h_{1k}(t) \right|^2}{h^2_{1(k-1)}(t)} \right] \tag{12}$$

Usually, a limit of 0.2–0.3 is set for SD. Moreover, the sifting process is stopped as long the last residual or the component becomes too small, a constant or a monotonic function.

The Hilbert transform is then evaluated for each obtained IMFs, to extract the instantaneous frequency, and afterwards the original data can be expressed by the following:

$$x(t) = \Re \left\{ \sum_{j=1}^{n} a_j(t) \mathrm{e}^{\left[ i \int \omega_j(t) dt \right]} \right\} \tag{13}$$

Which denotes a 3-D representation of the amplitude as a function of frequency and time, defined as Hilbert spectrum $H(\omega,t)$.

## 3. Damage assessment method

In the last decades different acoustic emission methods for structural damage assessment have been proposed. In [34] Gorman demonstrated the dispersive nature of the modes propagating in CFRP plate-like structures. Prosser et al. [52] analysed the modes generated from the impact test (high and low velocity) on aluminium and composites plates, observing characteristic damage features in the frequency domain. Mizutani et al. [53] studied the fracture mechanisms in carbon-fibre composites by analysing acoustic emission signals and compared them with symmetric and anti-symmetric modes produced with focused laser pulses. Early studies focused on the mode identification of the propagating wave field using specific signal processing methods [54,55]. Guo et al. studied the response of composite laminates to pencil-break test and pre-damaged samples subjected to tensile loading. Good agreement between the proposed theoretical solution of the wave motion and the experimental data was found in the frequency range of interest (2 MHz) [56]. Bourchak et al. developed a method based on the AE energy to evaluate the damage state of composite specimens subjected to static and fatigue loads. Results showed the capability of the method to evaluate the fatigue limit, the activity level of damage and damage accumulation threshold [57]. Eaton et al. [58] proposed a methodology to characterise damage based on the amplitude ratio of the main Lamb wave modes propagating in plate-like structures. The onset damage was effectively detected using the AE signals. In a recent study, a method relying on an estimation the arrival times of extensional and flexural waves by exploiting the wavelet decomposition has been proposed. Results from the decomposition could help understand the changes in propagation in case a damage occurred [59]. James et al. [60] developed a tool capable to identify impact events that generated damage, in real time, analysing the AE waveforms and relative spectrum, obtaining a characteristic AE signal signature that estimates whether a serious damage was induced within the composite structure. The methods presented above are effective to assess the integrity state of structures, but only as post-event process, i.e., that it's not feasible to evaluate the impact characteristics during the impact itself. Moreover, the described methods rely on a baseline, i.e., *a-priori* knowledge of the response of the structure in a pristine state to determine the specific features of an impact event is necessary. Additionally, the acoustic features whose these methods are based on are strongly affected by material properties, geometry, damage state, sensor layout and distance from the source [61]. Furthermore, some of the techniques are based on signal processing methods that are not suitable for non-linear and non-stationary data, the latter

typical characteristics of impact event signals. In order to overcome these limitations, a novel method based on the Hilbert-Huang transform of the decomposed wave field is proposed in this work. The use of the HHT in impact damage assessment brings the benefit of detecting type of impact by simply analysing the acoustic emission generated by the strike. Indeed, the HHT is capable to extract the different propagating modes (hence with different velocities) even in case where the modes are completely merged within the acquired signals. The proposed technique exploits the well-known capability of the HHT to extract meaningful real features from non-linear and non-stationary data. The damage feature is extracted by characterising the instant energies of the two main propagating modes, thus providing a real-time integrity state of the structure under inspection and discern elastic impacts from damaging one.

## 4. Materials and methods

### *4.1. Decomposition damage assessment method*

The initial stage of the proposed methodology for damage assessment includes the signal acquisition from a sensing network, which consists of a set of piezoelectric wafers active sensors (PWAS) properly coupled on the specimen or structure under inspection. The first step of the algorithm is to perform the empirical mode decomposition (EMD) of acquired signals, hence the acquired time series are processed retrieving the two main propagating modes (i.e., extensional and flexural), whose output is a set of intrinsic mode functions (IMFs). Since the decomposition is based on the local characteristic time scale of the data, this method specifically applies to non-linear and non-stationary data. The IMFs moreover admit well-behaved Hilbert transform. From the IMFs, mode separation is performed selecting the high-frequency components (extensional) from the medium–low frequency components (flexural) obtaining two separated signals.

The boundary between the two modes is evaluated with the frequency information embedded in each single mode function. For each IMF a routine evaluates the number of zero crossings and determine in which ratio the highest mode function has a higher frequency component than the lower modes. Consequently, higher the frequency component, higher is the number of zero crossings,

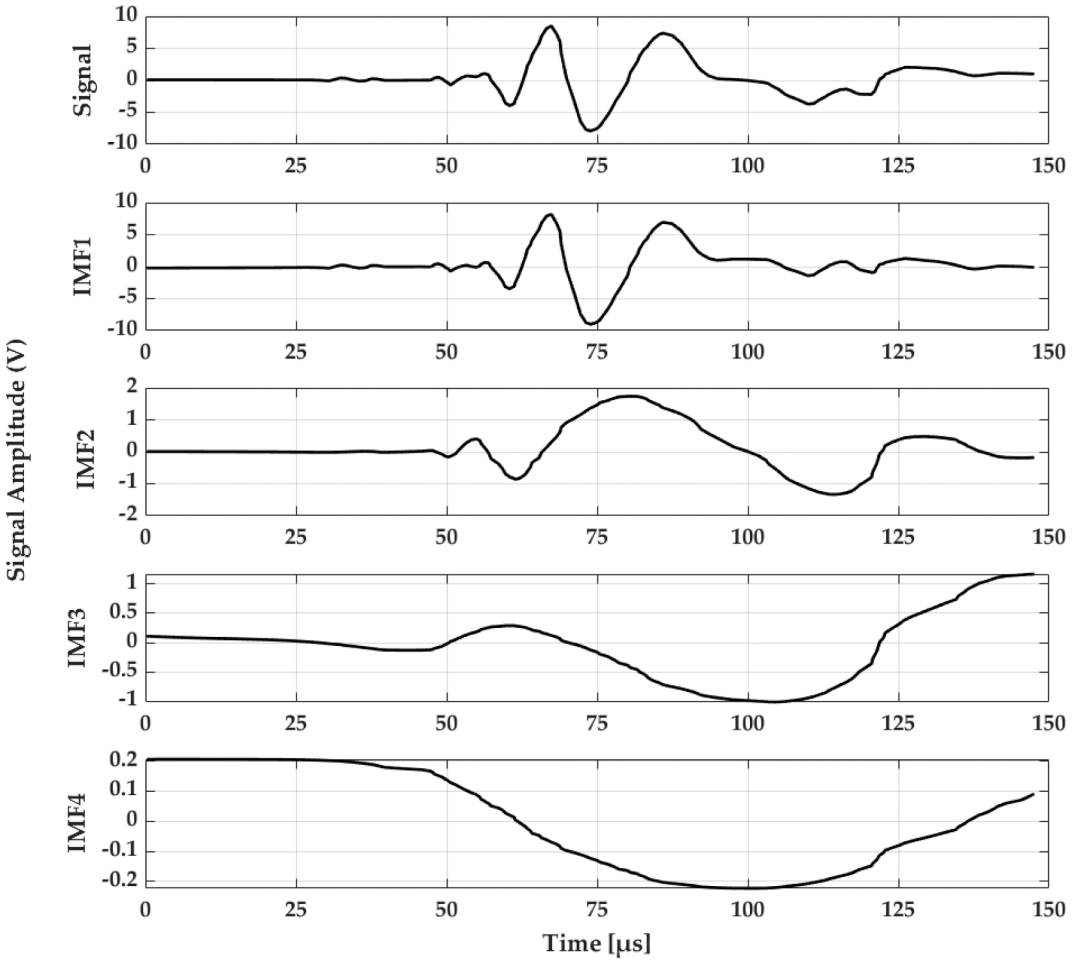


**Fig. 1.** Empirical mode decomposition and relative intrinsic mode functions.

leading to a clear discrimination between higher and lower frequency modes. The threshold between the modes is found to be highly reliant on the type of material, indeed in case of metals the extensional mode outperforms the flexural at least by a ratio of two while in cross-ply composites the extensional is about five time quicker than the flexural mode [3452]. In Fig. 1 the empirical mode decomposition of a signal from an impact performed on an aluminium plate, to demonstrate how the algorithm works.

The condition to evaluate the number of times the signals pass through zero is given by the following:

$$x_i < 0, x_{i-n} = 0, x_{i-N-1} > 0, with 0 \leq n \leq N$$

$$x_i > 0, x_{i-n} = 0, x_{i-N-1} < 0, with 0 \leq n \leq N \tag{13}$$

It is straightforward that the number of zero crossings is strictly linked with the wavelength of the propagating wave, hence the relation between the changing in sign of the signal with the frequency of propagation, considering known phase velocity values for conventional materials or cross-ply composites, is given by the following:

$$\lambda = \frac{c}{f} \tag{14}$$

where $c$ is the phase velocity of the extensional or flexural wave, and $f$ represents the frequency. Wavelengths in a ratio higher than a specific value defines the threshold between flexural and extensional waves, which propagate through structures with different phase velocity, usually in specific ranges depending on the material under examination [34,35,52,53], based on the premise that damaging impact can generate strong antisymmetric mode waves [62–64]. Hence, once set the threshold the two modes are then extracted.

A further step of the routine checks the quality of the lower frequency IMFs to be selected to reconstruct the flexural components of the signal. Indeed, during the empirical decomposition unwanted swings are generated at the begin and the end of the latest intrinsic functions, as shown in IMF4 in Fig. 1. This is caused by the spline interpolation through the extrema of the original signal during the sifting process. To avoid including these corrupted distortions, a cut-off is configured in the routine to remove those IMFs with very low energy content, one order of magnitude lower than the previous IMFs, that has little or no contribution to the signal and that are affected by large swings of the first and last part of the time series. Considering the IMFs from Fig. 1, the power distribution among the extracted components is represented in Fig. 2, and clearly shows that the IMF4 gives very low energy contribution to the whole signal, being one order of magnitude lower than the previous mode functions (threshold depicted in red) and affected by large variations. Hence, this mode function is excluded from the flexural component reconstruction of the propagating wave.

Finally, with the sorted and exact IMFs the extensional and flexural components are reconstructed respectively by linear combination, obtaining the two principal propagating waves through the structure, as depicted in Fig. 3, for the decomposition example of Fig. 1 above.

Afterwards, the Hilbert-Huang transform is executed on these two reconstructed signals, obtaining the Hilbert spectrum $H(\omega,t)$ for the extensional and flexural modes. From the instant energy information retrieved from the previous calculation, the damage descriptor $\Xi$ is determined, by the following:

$$\Xi = \frac{E_{i,max,extensional}}{E_{i,max,flexural}} \tag{15}$$

The parameter $\Xi$ can efficiently and properly describe the intrinsic features of the impact occurred on the inspected structure. Indeed, analysing how the instant energy is distributed between flexural and extensional modes, and considering how this is affected by the generation or not of a damage or failure, an information on the health state of the inspected component can be easily retrieved. Values of $\Xi$ between 0 and 1 are a sign of low probability of damage. For values of the parameter tending towards one there is a probability of small indentation of the structure. When the $\Xi$ parameter is reaching values higher or much higher than 1, penetration

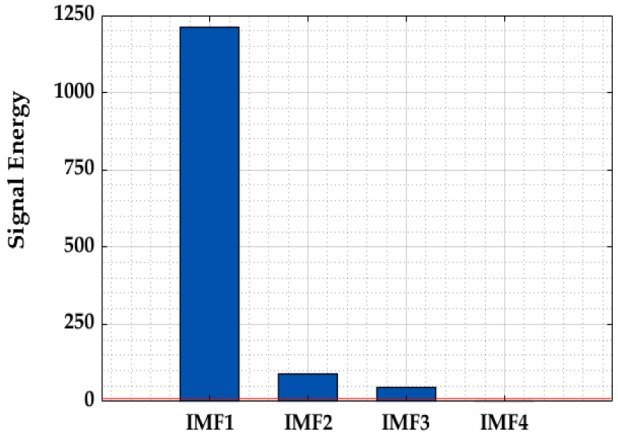


**Fig. 2.** Energy levels and threshold.

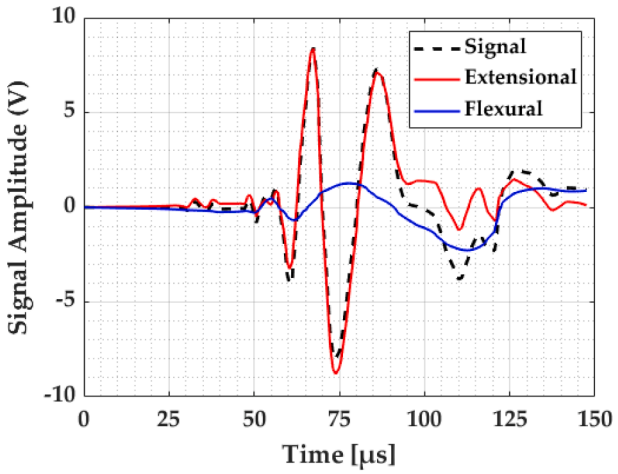


**Fig. 3.** Extracted extensional and flexural components.

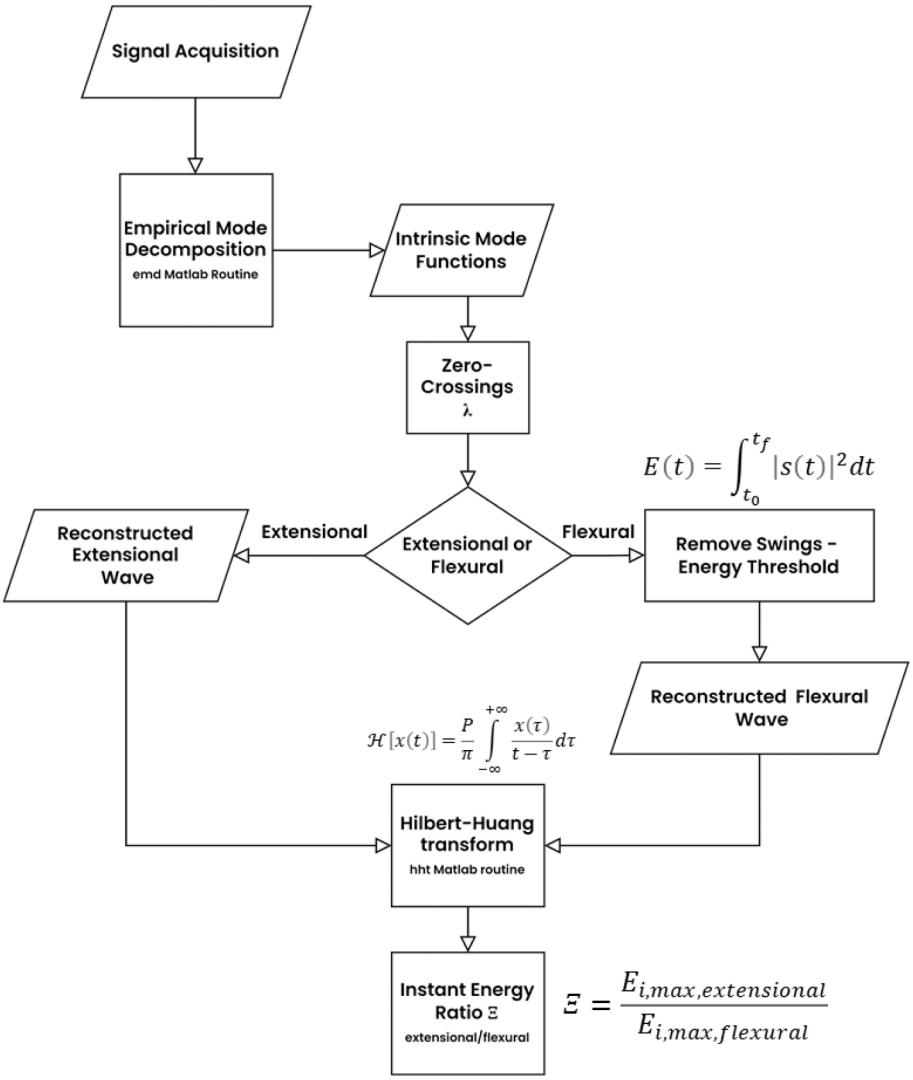


**Fig. 4.** Damage assessment method (block scheme).

and perforation of the structure is likely to occur because the extensional component in this scenario is dominant than the flexural one [52]. The uniqueness of the new tool is its capability to discern in real-time elastic and damaging impacts without the requirement of baseline datasets.

Hereafter, in Fig. 4, a detailed scheme of the method, with full description of the steps required to determine the proposed damage descriptor $\Xi$.

The experimental campaign executed to validate the proposed method included four setups, with specimen and samples made of aluminium or different types of composite materials. Furthermore, different types of impact were performed, in terms of velocity or energy and in terms of different type of impactor or rig used. This diversification was opted by the authors to demonstrate the method capabilities in multiple scenarios. It's worth remember the most common classification of the different impact based on velocity range. Until 10–20 m/s it is usually referred as low velocity impact (LVI) and until 50 m/s as intermediate impact; from 50 m/s till 1000 m/s are defined as high velocity impact (HVI), and above 2 km/s are considered hyper velocity or ballistic impact [6,65,66]. The output results from the experimental campaign are meant to prove the expected trend of the energy ratio $\Xi$ introduced and discussed before and based on the wave field propagation theory in plate-like structures, generated by impact. Results are expected to show that as long as a permanent deformation or damage are induced into the structure the energy ratio should increase in value, according to the modifications in the modes embedded in the wave field. Indeed, as demonstrated and proved in literature (referenced in previous sections) different types of damage are related to different propagating modes.

### 4.2. Setup 1: High and hyper velocity impact on aluminium Plate.

A 0.5x0.5 m 3 mm thick aluminium plate subjected to medium–high and high-velocity impact was used for Setup 1. With this regard, the impact was performed by means of an airgun shooting a spherical steel projectile with diameter of 4.5 mm for the first two tests, and nylon cylinder with 1.5 mm diameter for the high velocity-one [52].

Three impact tests were executed, at three different velocities, the first two at 0.04 km/s and 0.1 km/s for the medium–high velocity range and 4 km/s for the high velocity impact. A sensing network composed of three broadband sensors, with central frequency of 300 kHz, was attached to the surface of the plate, to acquire the signals generated by the impact. All the signals for the medium–high velocities were sampled at 2 MHz, while the last test was digitised with a sampling frequency of 10 MHz [52]. The samples were firmly attached with stainless steel fixture. A schematic representation of the experimental setup is pictured in Fig. 5.

### 4.3. Setup 2: Hyper velocity impact on CFRP Plate.

In the second experimental setup two CFRP square plates were considered. The first with dimensions of 0.3 by 0.3 m and 1.2 mm thickness and plies, the second with 0.4 by 0.4- and 2.5-mm thickness and 24 plies, both tested at high velocity impact, executed with an air gun shooting cylindrical nylon projectiles. Three impact tests were conducted, at three velocity levels, at 2 km/s, 5.2 km/s and 6.6 km/s. A sensing network with four sensors was used to acquire the signals from the impact events, which in turn were digitised with a sampling frequency of 10 MHz [52]. Throughout the tests performed the samples were properly attached with a specific fixture. In Fig. 6, a schematic representation of the samples and the test setup.

### 4.4. Setup 3: Medium-High velocity impact on CFRP stiffened panel.

The third experimental setup configuration considered a CFRP *T*-stiffened panel, extracted from an actual airplane wing structure. Four tests were performed on the same specimen, at four different velocity levels: 0.04 km/s, 0.05 km/s, 0.06 km/s and 0.07 km/s using a custom air gun, and spheric steel projectiles. The sensing network was constituted of three piezo sensors with central frequency of 300 kHz, and the sampling frequency was set at 2 MHz for the acquisition of data (see Fig. 7).

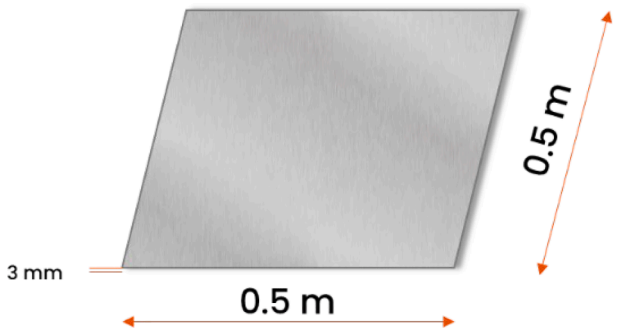


**Fig. 5.** Experimental setup 1.

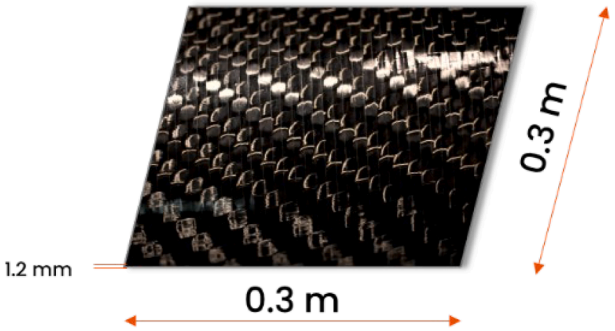


**Fig. 6.** Experimental setup 2.


**Fig. 7.** Experimental setup 3.

### 4.5. *Setup 4: Low velocity impact test on pre-damaged CFRP sample.*

The fourth and last experimental setup examined a pre-damaged 150x100 mm, 2 mm thickness, 11 cross-ply CFRP sample. The impact tests were performed with an impactor rig, according with ASTM D7136 [67],with anti-rebound system to avoid multiple impacts. The falling shuttle impacting the samples included a steel spherical tip with 10 mm diameter. Two piezo sensors were attached to the sample to acquire test signals, one located underneath the impact point, on the outer face of the sample, and the second

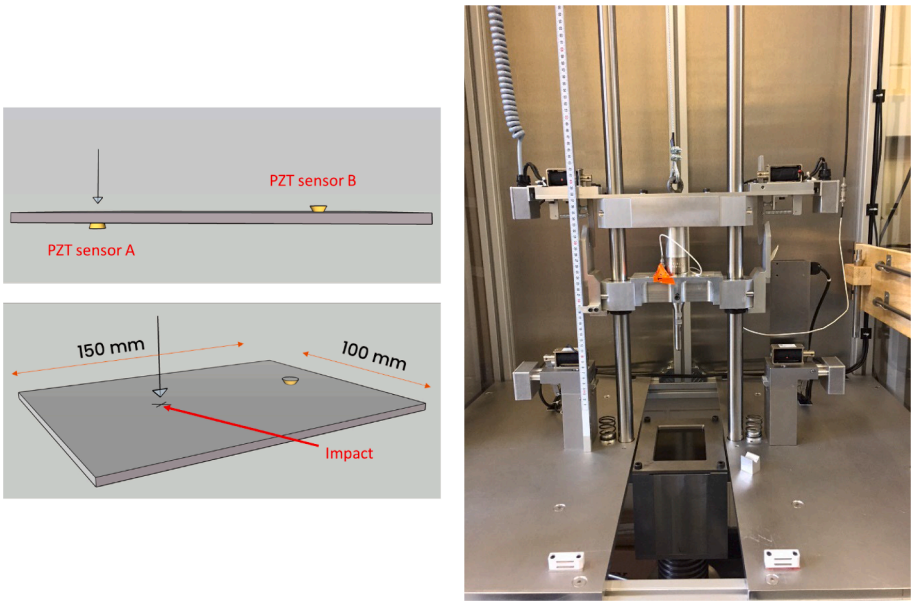


**Fig. 8.** Experimental setup 4.

located far from the impact point. The acquired signals were digitally converted at 2 MHz sampling rate. Two impacts were performed on the same specimen, the first at a level (release height equal to 50 mm) that generated no further damage, and the second at a level (release height equal to 200 mm) that generated visible damage to the sample. A schematic representation of the experimental setup and the sample is shown in Fig. 8.

## 5. Results and discussion

In this section, all the results from the experimental campaign are introduced and then discussed, highlighting the most important insights obtained. All the results are divided per experimental setup as presented in chapter 4.

### 5.1. Setup 1

The impact executed on the aluminium plate generated no perforation in any of the three test scenarios, with small indent in the high velocity range and huge deformations for the hyper velocity impact. In Fig. 9 hereafter, the signals from the three-impact test with relative velocities.

Fig. 9 showed how the signal propagation changes accordingly with the impact velocity.

In the first two impact within the location where the projectile stroke the plate, a considerable indentation with no perforation was generated. In these two cases, the extensional mode has low amplitude, and the wave field is mainly constituted by the flexural component. In the third case, i.e., hyper velocity impact, the impact generated a larger deformation but still without perforation. The acquired signal clearly depicted the extensional part, with higher frequency components, with amplitude comparable with the high frequency range of the flexural mode. Moreover, a decomposition of the three signals in the two fundamental modes have been performed by means of the proposed algorithm. The Hilbert spectrum plots for the three different impact velocities are depicted in the Figs. 10-12, where the different energy distribution of flexural and extensional modes in time and frequency domain are shown.

It's interesting to observe from the spectrum above the distribution of the energy content in the signal recorded, showing the modification of the dominant mode when the velocity is increased. Indeed, in Fig. 12, the highest energy values are in the extensional part at higher frequencies, as expected for this mode.

Values of $\Xi$ for all the scenarios considered for the experimental setup are shown in Fig. 13.

From the output of the Hilbert spectrum, the damage descriptor $\Xi$ is calculated using the equation introduced in section 3.1. Fig. 13 shows the $\Xi$-coefficient for all the scenario, where it becomes apparent that, for high-velocity impacts, the damage descriptor has value towards zero, i.e., no damage occurred in the impact event. Instead, the damage descriptor reaches value towards one in case of non-perforating impacts with onset damages, i.e., penetration or considerable deformations. This behaviour is well explained by the modification of the propagating modes; indeed, the extensional components are neglectable compared to the flexural ones for high velocity impact, meanwhile in the hyper velocity the energy of the extensional waves is comparable to the one of the prevalent flexural components. $\Xi$ tends to zero for non-perforating impacts where only small indents are induced, while approaches one for impacts inducing large deformations and penetration. This behaviour is in agreement with the discussion in section 4.

### 5.2. Setup 2

The impacts on the composite plates were executed at hyper velocities, which the first caused no perforation, and the other two induced perforation of the structure. The acquired signals for the three impacts and relative velocities are shown in Fig. 14.

In the first plot in Fig. 14 (i.e., impact velocity 2 km/s), the flexural component is predominant compared to the extensional one, but both are clearly excited by the impact, with the extensional characterised by higher frequency. The amplitudes of the two modes are almost comparable, as visible in Fig. 14. Increasing the impact velocity to a level that induced penetration of the sample, the propagation modes changed, and the extensional component becomes predominant, while the flexural part decreased substantially. This trend is consistent in both impact with penetration, as depicted in Fig. 14, in the plot related to these two impacts. Performing the damage analysis with the new technique, the decomposition in the extensional and flexural components of the impact signals is achieved. The energy distribution in frequency and time, between the fundamental modes propagating within the impacted samples, and how this distribution changes in function of the impact characteristics is shown in Figs. 15-17.

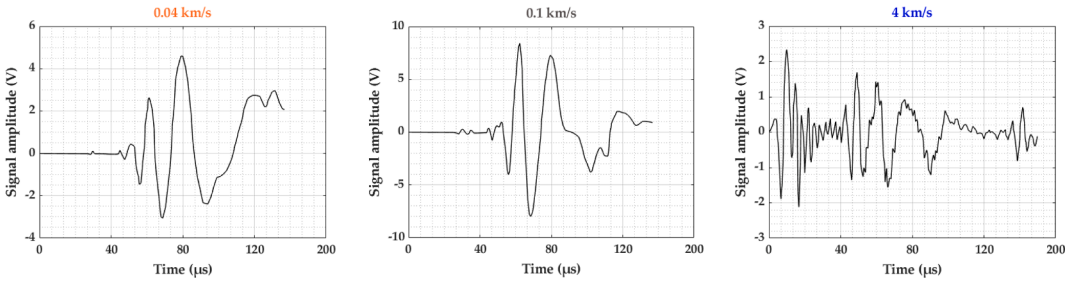


**Fig. 9.** Signals acquired from impact test on aluminium plate.

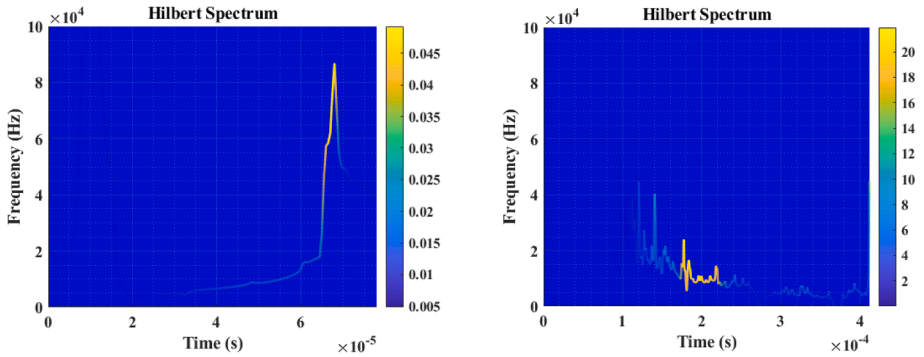


**Fig. 10.** Hilbert spectrum of the extensional (left) and flexural (right) modes from the impact at 0.04 km/s.

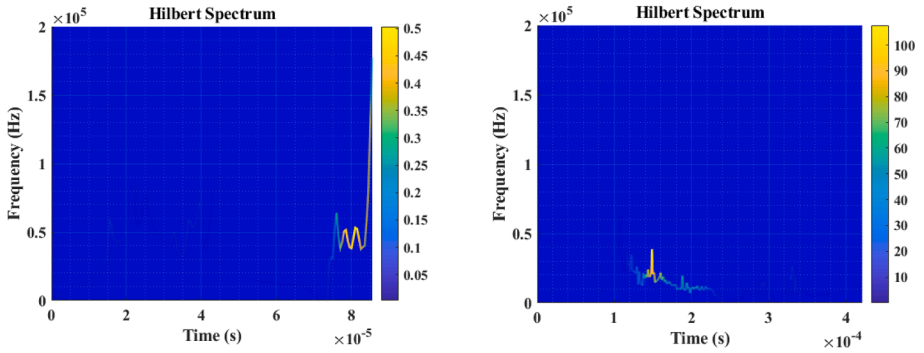


**Fig. 11.** Hilbert spectrum of the extensional (left) and flexural (right) modes from the impact at 0.1 km/s.

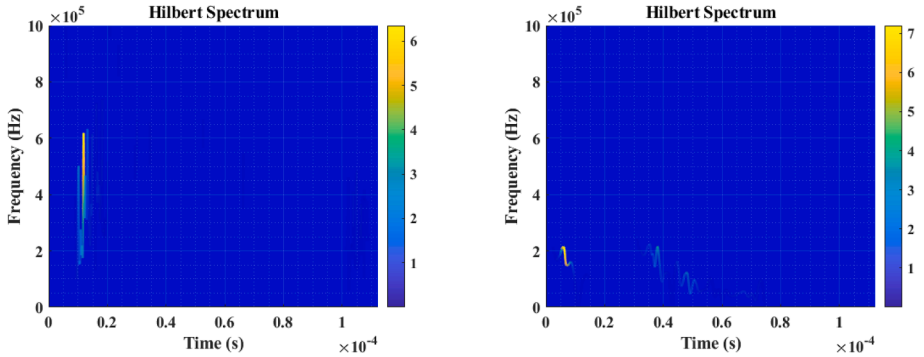


**Fig. 12.** Hilbert spectrum of the extensional (left) and flexural (right) modes from the impact at 4 km/s.

It's very interesting the distribution of the instant energy from the figures above. In all the impact performed in this setup the extensional mode is dominant, with increasing instant energy as the impact velocity is increased, while the flexural part is stable to similar values in all scenarios. It's worth to observe the clear difference of frequency content between the two main modes, with higher values for the extensional, in accordance with literature.

From the output data of the evaluated Hilbert spectrum, the damage descriptor Ξ was calculated, and reported in the Fig. 18.

In the first test, the Ξ-parameter is around one, which means that the two modes have similar contribution, and no visible relevant damage is induced to the specimen unless indentation and fibre breakage of the top layers. This is in good agreement with the high velocity test performed on the aluminium plate in the previous section. When the impact velocity is increased until perforation of the specimen occurred, Ξ reaches values above one, because of the modification of the propagating modes. Indeed, in this case, the predominant component is the extensional one, as shown in Fig. 16 and Fig. 17. Hence, the increasing trend of the damage descriptor Ξ (+350 %) are related to the generation of full damage of the structure, which is in good agreement with literature stating that for perforation, the flexural component is barely present, and the predominant component is extensional. It is possible to conclude that as the damage descriptor Ξ reaches values larger or much bigger than one full damage or perforation of the structure had occurred and

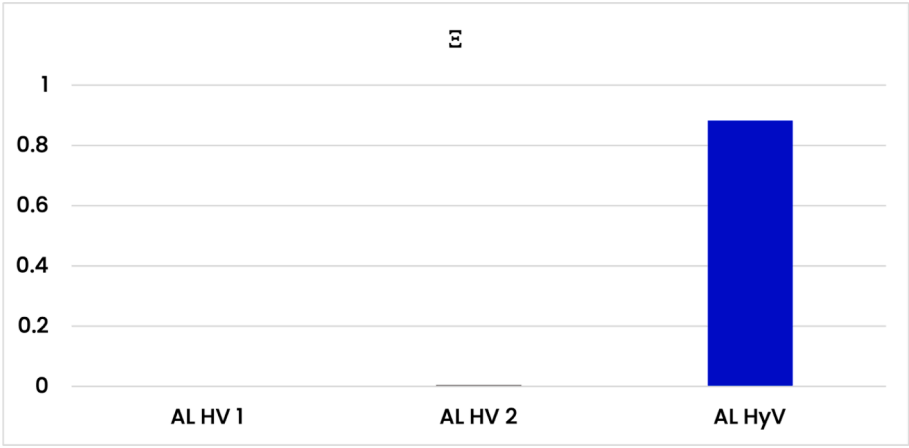


**Fig. 13.** Ξ values for the three impact tests on aluminium plate.

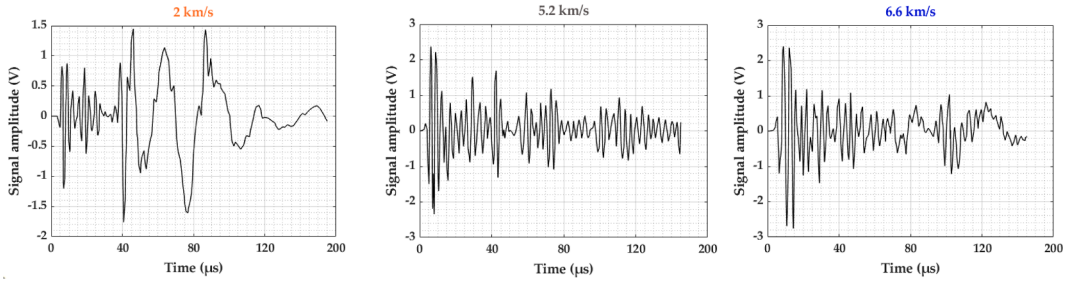


**Fig. 14.** Signals acquired from impact test on composite plate.

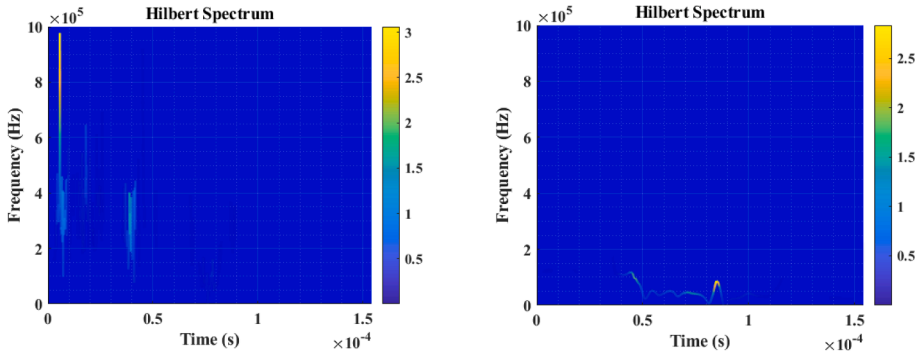


**Fig. 15.** Hilbert spectrum of the extensional (left) and flexural (right) modes from the impact at 2 km/s.

can be used as a reference parameter to assess the health state of the monitored structure.

### 5.3. Setup 3

The impact test was executed on the CFRP stiffened panel to evaluate the flexibility of the proposed method to ascertain the damage state in complex structures. The effects of the impact executed on the stiffened panel are illustrated in Fig. 21, where only two impact induced visible damage to the panel, with fibre breakage and top layer delamination. Phased Array Ultrasonic Testing (PAUT) inspections were also conducted to visualise internal damages occurred after impact events. On this matter, C-Scans illustrating the amplitude and travelled distance (Time-of-flight) of the propagating ultrasonic wave into the test-sample, are shown in Fig. 21, in such a way that a planar view of internal state of the specimen and penetration can be visualised. Moreover, the signals acquired from the two central piezo sensors (close to the impact area) were out of scale, due to the intensity of the impact, hence only signals from the far located sensor were analysed. Hereafter, the signals from the four-impact are shown in Figs. 19-20.

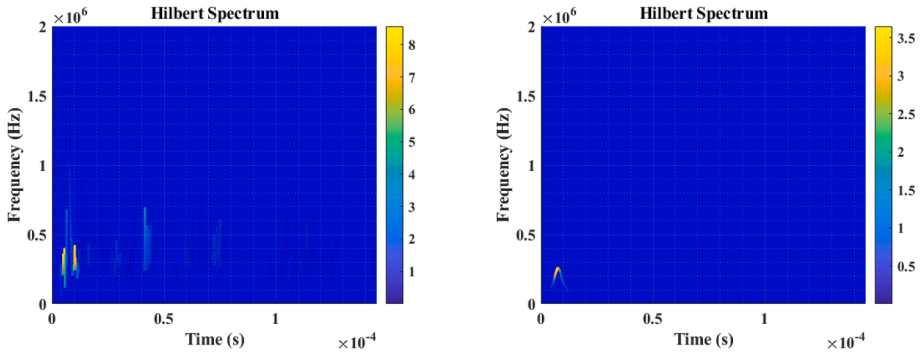


**Fig. 16.** Hilbert spectrum of the extensional (left) and flexural (right) modes from the impact at 5.2 km/s.

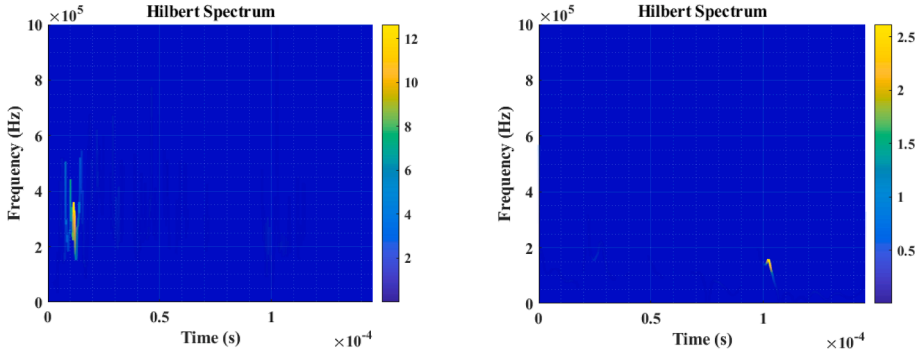


**Fig. 17.** Hilbert spectrum of the extensional (left) and flexural (right) modes from the impact at 6.6 km/s.

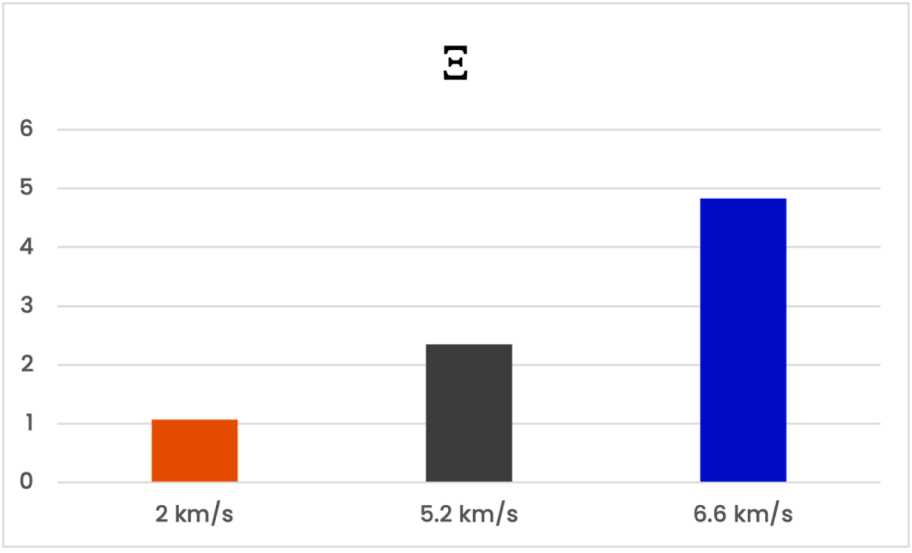


**Fig. 18.** Ξ values for the three impact tests on CFRP plate.

Results showed a high frequency component within the signals, due to the higher rigidity of the specimen considered. Additionally, the extensional and flexural modes are more combined, compared to the signals from the previous setup. In terms of amplitude, it is clear how the overall amplitude of the propagating modes is increased consistently as the impact velocity increases. Performing the damage analysis with the developed method, the two fundamental modes are retrieved, and afterwards the Hilbert spectrum are evaluated.

As visible from Figs. 21-22, impact 3 and 4 generated visible damage on the top surface of the sample, with clear fibre breakage. The

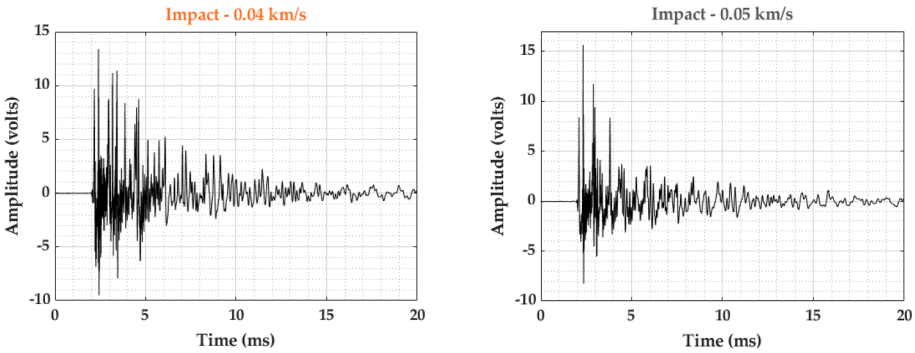


**Fig. 19.** Signals acquired from impact at 0.04 km/s and 0.05 km/s.

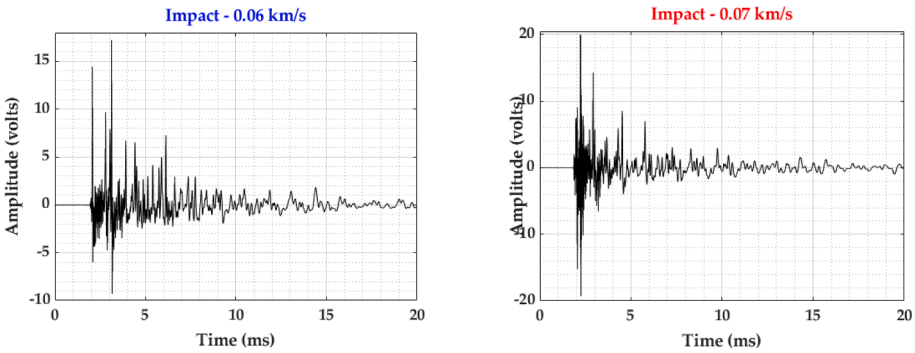


**Fig. 20.** Signals acquired from impact test at 0.06 km/s and 0.07 km/s.

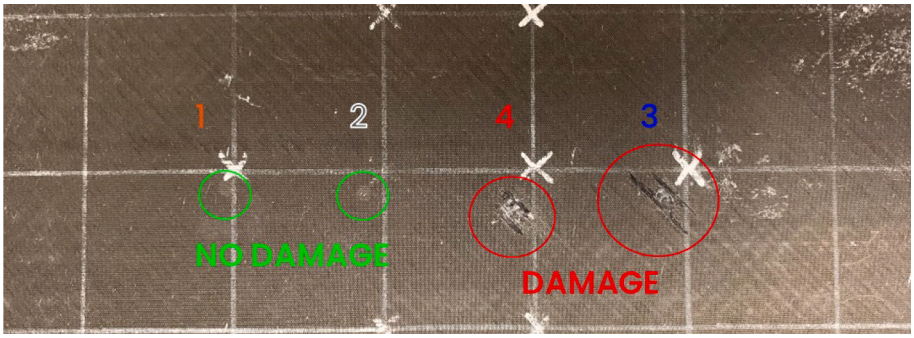


**Fig. 21.** Visual inspection of the damage induced to the stiffened panel.

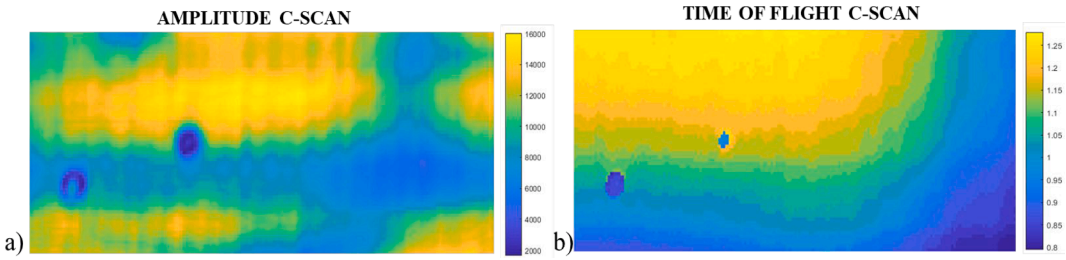


**Fig. 22.** PAUT results for the stiffened panel; a) Amplitude C-Scan imaging; b) Time of Flight imaging.

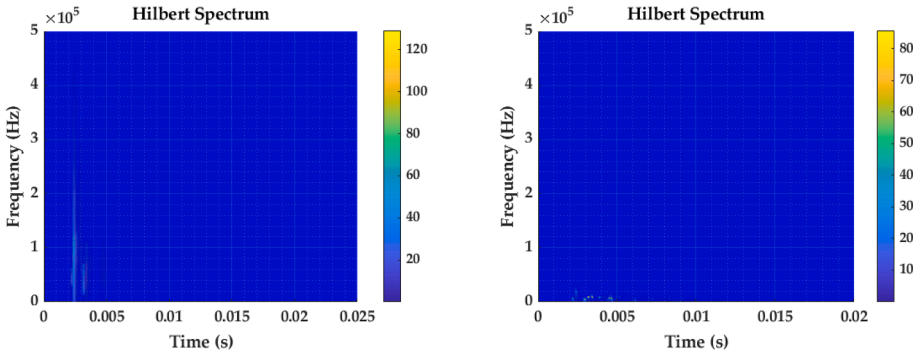


**Fig. 23.** Hilbert spectrum of the extensional (left) and flexural (right) modes from the impact at 0.04 km/s.

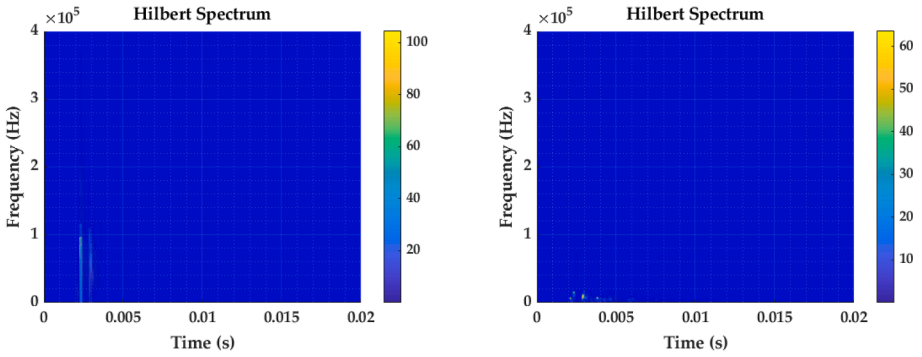


**Fig. 24.** Hilbert spectrum of the extensional (left) and flexural (right) modes from the impact at 0.05 km/s.

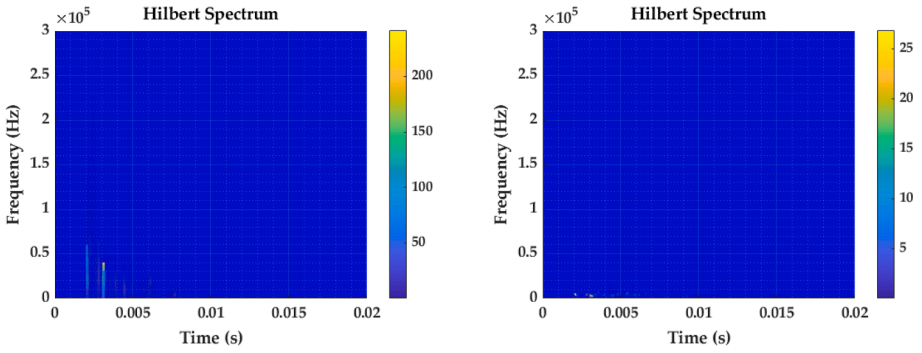


**Fig. 25.** Hilbert spectrum of the extensional (left) and flexural (right) modes from the impact at 0.06 km/s.

Hilbert spectrum for all the four tests executed are reported in the following figures (Figs. 23-26).

As shown in Figs. 25-26, the higher frequency extensional components are separated from the low-frequency flexural ones. The energy distribution changes as a function of the impact velocity and for eventual damage induced by the impact itself. The highest frequency values are all related to the extensional modes, carrying most of the energy content as well. It's worth noting in this scenario that the flexural part is not much lower than the extensional, as observed in the previous setups. This is mainly due to the different type of geometry tested, which in turn have a different response to the impact excitation. From the output data of the Hilbert spectrum (instant frequency and energy) the damage descriptor Ξ was evaluated and reported in the bar plot illustrated hereafter in Fig. 27.

The trend observed for the Ξ parameter is consistent with the behaviour analysed in the previous experimental setups. For the first two impact, at 0.04 km/s and 0.05 km/s, no visible damage was detected on the top surface of the panel apart from small indents and this is reflected by the damage descriptor with values slightly above one, due to an extensional component marginally higher than the flexural one even though no major damage occurred. In this case, the extensional and the flexural components are characterised by quite similar intensities, without a predominant mode, according with the trend observed in the previous tests analysed. For the impact at 0.06 km/s and 0.07 km/s, the values of the damage descriptor are considerably higher than unit, around 4 and 9 respectively. This

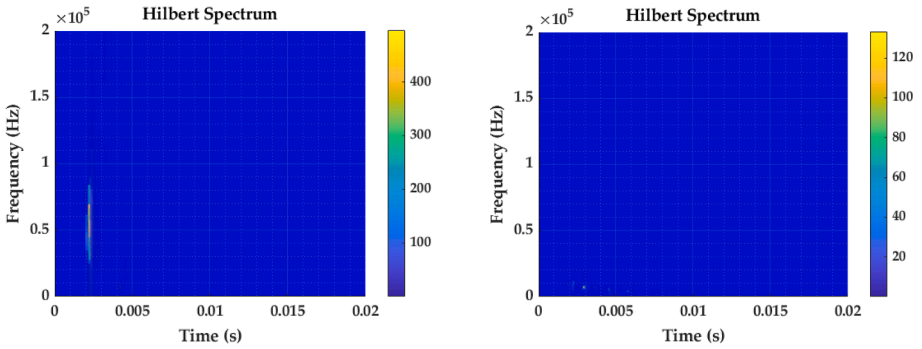


**Fig. 26.** Hilbert spectrum of the extensional (left) and flexural (right) modes from the impact at 0.07 km/s.

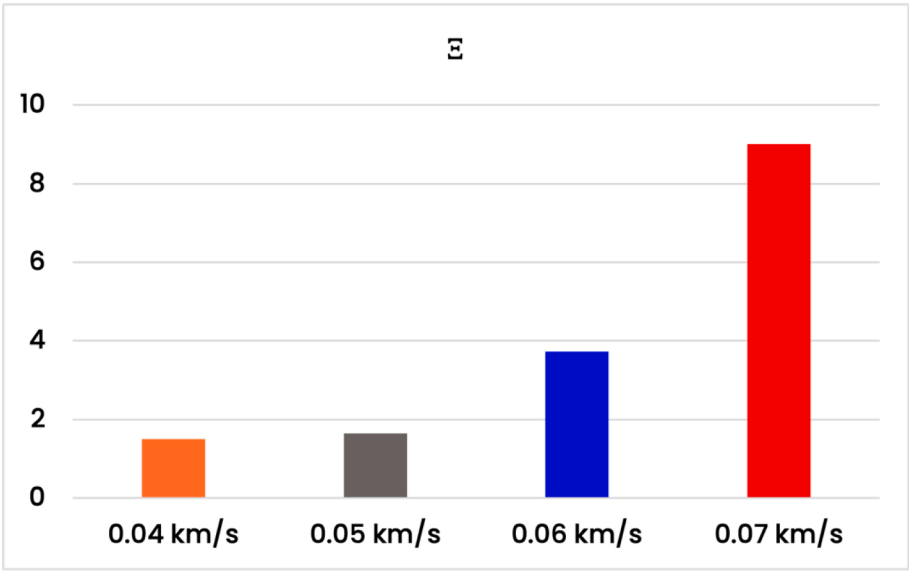


**Fig. 27.** Ξ values for the four impact tests on stiffened panel.

translates to an extensional mode being predominant in the propagating wavefield, relatable to induced damage to the structure, in accordance with the PAUT inspections conducted on the sample, as consistently visible in Fig. 21. In agreement with literature and the scenarios observed in previous sections, the extensional component becomes predominant as damage occurs, and the instant energy is mainly distributed upon this mode. Hence, it is evident that the proposed method can provide damage assessment for more complex structure as well.

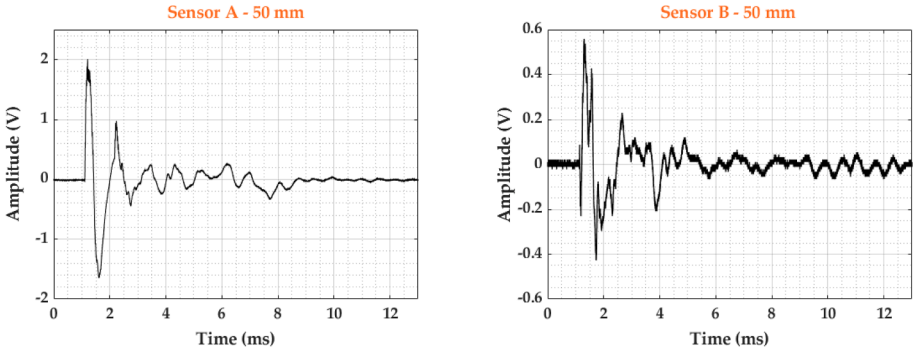


**Fig. 28.** Signals from the 50 mm impact: Sensor A (left) and Sensor B (right).

### 5.4. Setup 4

The tests performed on the CFRP sample were conducted to evaluate the performance of the method in the case of signals acquired from a pre-damaged structure, and how this can affect the estimation of the damage state with the proposed parameter Ξ. A schematic illustration of locations for previous and further impacts is shown in Fig. 30. C-scan imaging in Fig. 31 showed the typical complex nature of the low velocity impact (LVI) damage in CFRP structures [68,69], as well as further damage occurred after the second LVI. The signals acquired from the two piezo sensors (under the impact location and far from the impact) were both considered for the damage estimation using the method. The signals acquired from the two impact tests are illustrated in Figs. 28-29.

The two main propagation components were then decomposed, and afterwards the damage analysis was executed whose output is the Hilbert spectrum for each mode, and each sensor. As shown in Figs. 28-29, the signal amplitudes increase for higher energy impact, with higher frequency components embedded. The Hilbert spectrum for all the configurations is evaluated and shown in Figs. 32–35.

The Hilbert spectra in Figs. 32-35 reveal the instant energy distribution evaluated from sensor A and B for the different impact velocities, with a change in the modes component as further damages are induced in the sample. These figures highlight that the wave modes on a pre-damaged plate have different behaviour than a pristine sample. Indeed, the first impact LV1 is not causing further damage and the flexural components is prevalent than the extensional, as observed in previous tests. The impact LV2 induced further damage to the sample, but in this case the extensional component is not becoming similar or dominant than the flexural one. This is main due to the modified stiffness caused by the previous damage; hence the response of the second damaging impact is not similar to the response of the previous tests. The damage descriptor Ξ was then evaluated for each impact (See Fig. 36), which shows a different trend compared to previous setups, as expected from the analysis of the Hilbert spectrum. Indeed, Ξ-coefficient is lower than one in both the scenarios (0.37 and 0.7 for sensor A, 0.1 and 0.4 for sensor B), which means the flexural component is still predominant, although the sample is already damaged. Despite this different trend, the most interesting insight is that as further damage was induced to the sample with the second impact, leading to perforation, the damage descriptor Ξ is doubled (+94 and + 290 % for sensor A and B respectively) compared with the first impact. This means that even though the damage descriptor does not follow the trend expected, due to the presence of the pre-damage that causes a different mode propagation, the introduced parameter is still able to identify an increase in the damage state, in this case full fracture, of the sample due to an increase in the extensional component for higher energy impact. Also, this variation in the propagation modes is probably due to the impact mechanism, since the impacts have been executed with the impactor rig, thus leading to much higher flexural displacement according with the boundary conditions. hence can be expected that in this type of tests the flexural component is more predominant than the extensional.

Nevertheless, the method could still be able to detect a change in the state of the sample when further damage was induced, proving the capabilities of the proposed technique, as well as good feedback on the health conditions of the structure.

## 6. Conclusions

In this work, an alternative and baseline-free real time SHM approach was proposed to provide damage feedback during an impact event. The method evaluates the occurrence of damage by the decomposition of the Lamb waves by means of the Hilbert-Huang transform. Four different setups with different impact scenarios and specimen were considered to assess the effectiveness of the damage descriptor parameter Ξ defined in this work as the ratio between the maximum instant energy of the extensional mode and the maximum instant energy of the flexural mode. For the aluminium case, as long as no damage is induced to the structure, Ξ is lower than one in case where no large deformation occurred, and approaches unity in the high velocity impact when considerable plastic deformations affected the sample. For the CFRP plate, Ξ-coefficient assumed value around one, due to the presence of small flaws induced after the impact. As perforation occurred for the high velocity impact, Ξ reaches values higher than one (around 2.5 and 5 for the two impact respectively). This trend was confirmed by the test executed on the stiffened panel, where impact at the highest velocities showed large Ξ values (around 4 and 9 at 0.07 km/s and 0.06 km/s respectively), when visible damage was occurred. Hence, When the Ξ parameter is reaching values higher or much higher than 1, penetration and perforation of the structure is likely to occur, because the extensional component in this scenario is more dominant than the flexural one. In case of an existing damage, despite a change in the

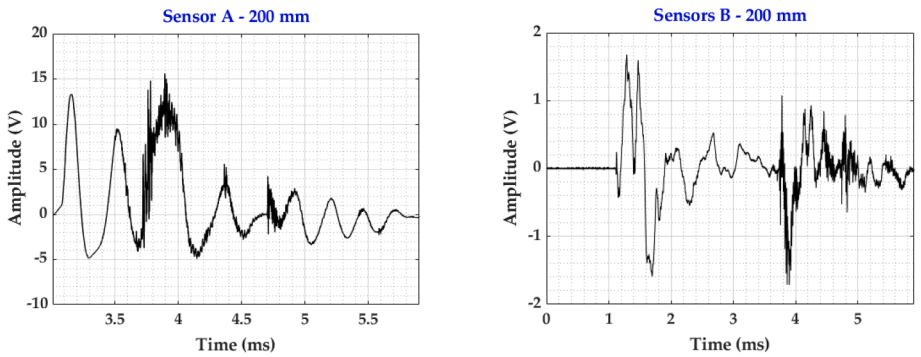


**Fig. 29.** Signals from the 200 mm impact: Sensor A (left) and Sensor B (right).

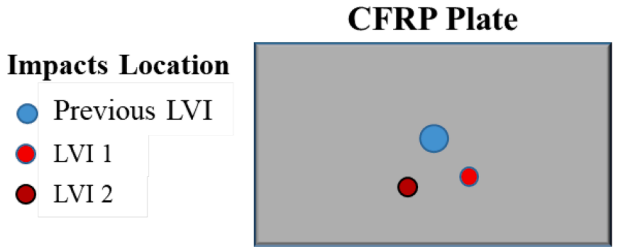


**Fig. 30.** Schematic representation of impact locations for setup.

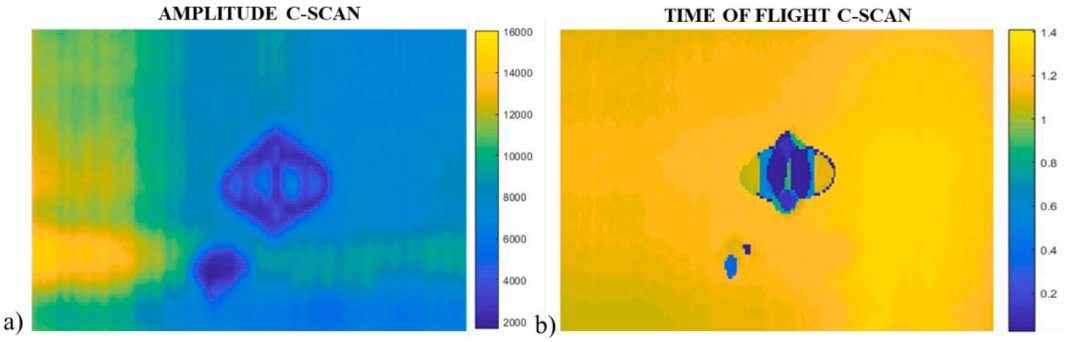


**Fig. 31.** PAUT results for pre-damaged CFRP plate; a) Amplitude C-Scan imaging; b) Time of Flight imaging.

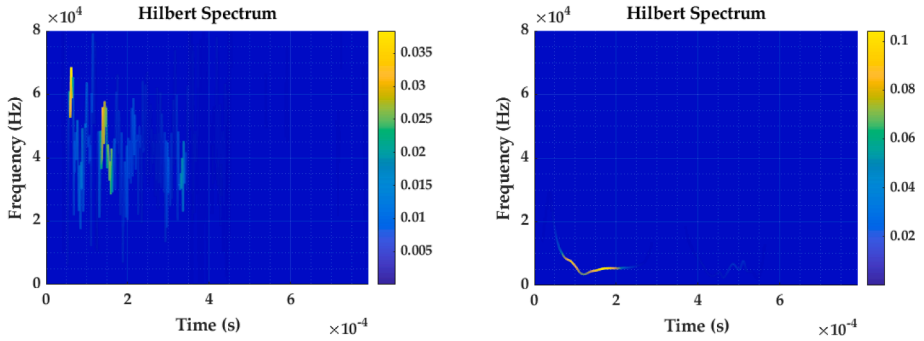


**Fig. 32.** Hilbert spectrum of the extensional (left) and flexural (right) modes from the impact at 50 mm Sensor A.

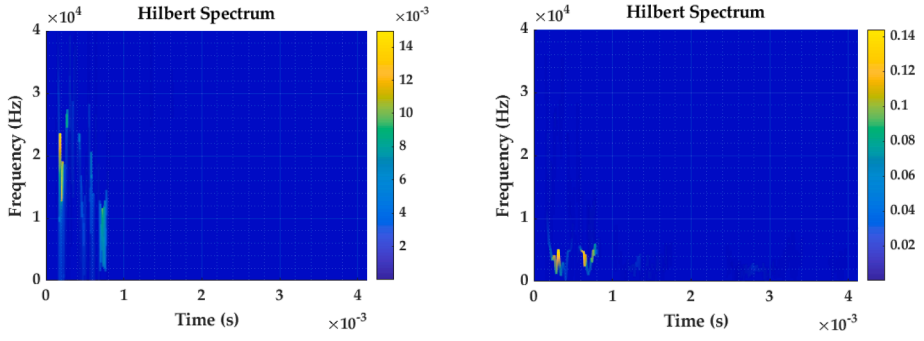


**Fig. 33.** Hilbert spectrum of the extensional (left) and flexural (right) modes from the impact at 50 mm Sensor B.

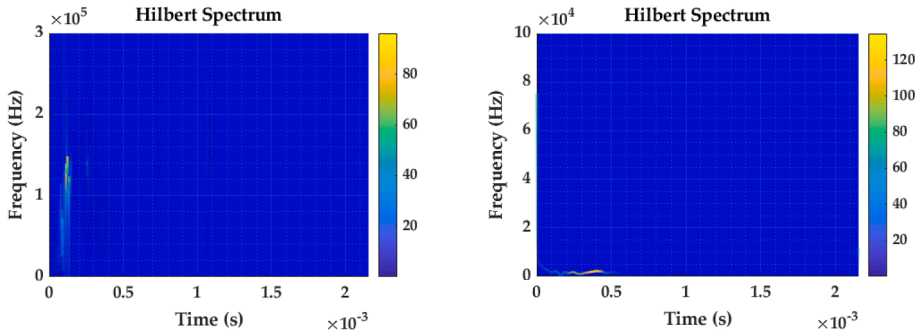


**Fig. 34.** Hilbert spectrum of the extensional (left) and flexural (right) modes from the impact at 200 mm Sensor A.

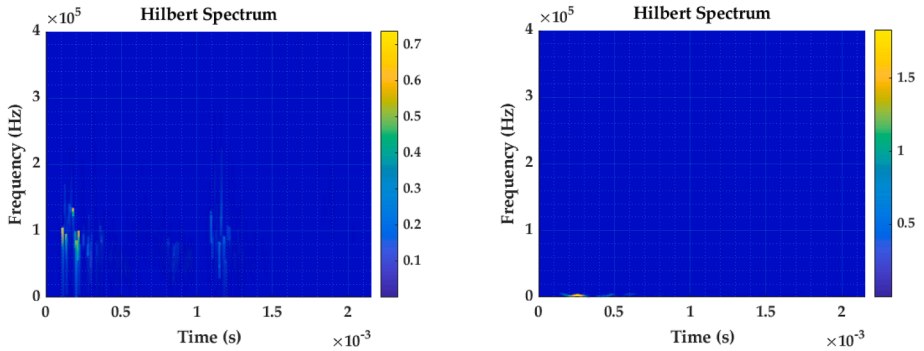


**Fig. 35.** Hilbert spectrum of the extensional (left) and flexural (right) modes from the impact at 200 mm Sensor B.

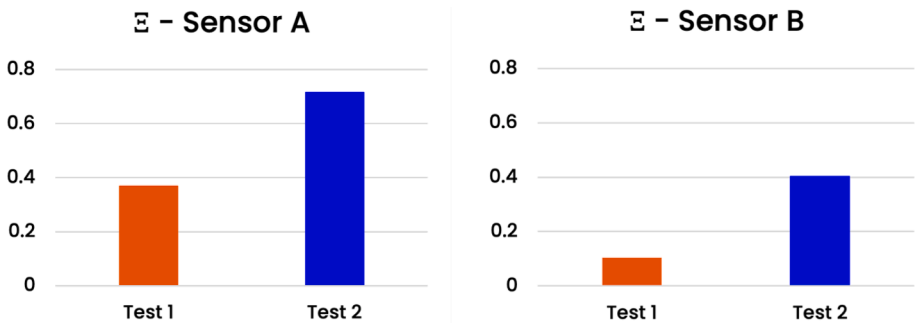


**Fig. 36.** Ξ values for the impact on the pre-damaged CGRP sample for Sensor A (left) and Sensor B (right).

trend of Ξ compared to previous tests, the method could identify full fracture of the specimen, where an increment in the damage state occurred (+94 % of Ξ). In conclusion, the method introduced in this work could represent a valuable way to assess the creation of damage state into a structure, in real time and more significantly with no needs of a baseline dataset, as existent methods in literature.

## Declaration of Competing Interest

The authors declare that they have no known competing financial interests or personal relationships that could have appeared to influence the work reported in this paper.

## Data availability

No data was used for the research described in the article.

## References


[1] "Guidelines for Implementation of Structural Health Monitoring on Fixed Wing Aircraft." SAE, 2013. [Online]. Available: https://saemobilus.sae.org/content/arp6461.
[2] C.R. Farrar, N.A.J. Lieven, Damage prognosis: The future of structural health monitoring, Philosoph. Trans. Roy. Soc. A: Mathemat. Phys. Eng. Sci. 365 (1851) (2007) 623–632.
[3] D. Cristiani, C. Sbarufatti, M. Giglio, Damage diagnosis and prognosis in composite double cantilever beam coupons by particle filtering and surrogate modelling, Struct. Health Monit. 20 (3) (2021) 1030–1050, https://doi.org/10.1177/1475921720960067.
[4] M. Grasso, F. Penta, G.P. Pucillo, F. Ricci, V. Rosiello, Low velocity impact response of composite panels for aeronautical applications, Lecture Notes in Eng. Comput. Sci. 2218 (2015) 1138–1143.
[5] S. Cuomo, F. Rizzo, G. Pucillo, F. Pinto, M. Meo, A thermoplastic polymer coating for improved impact resistance of railways CFRP laminates. In ECCM 2018–18th European Conference on Composite Materials, 2020.
[6] S. Abrate, Impact Engineering of, Compos. Struct. (2011), https://doi.org/10.1007/978-3-7091-0523-8.
[7] M. Capriotti, H.E. Kim, F.L.d. Scalea, H. Kim, Non-destructive inspection of impact damage in composite aircraft panels by ultrasonic guided waves and statistical processing, Materials 10 (6) (2017) 616.
[8] M.J. Santos, J.B. Santos, A.M. Amaro, M.A. Neto, Low velocity impact damage evaluation in fiber glass composite plates using PZT sensors, Compos. B Eng. 55 (2013) 269–276.
[9] M. Gresil, L. Yu, V. Giurgiutiu, Fatigue crack detection in thick steel structures with piezoelectric wafer active sensors, Nondestruct. Characteriz. Compos. Mater., Aerosp. Eng., Civil Infrastruct. Homeland Secur. 2011 (2011), https://doi.org/10.1117/12.882137.
[10] M. Gresil, V. Giurgiutiu, Guided wave propagation in composite laminates using piezoelectric wafer active sensors, Aeronaut. J. (2013), https://doi.org/10.1017/S0001924000008642.
[11] M. Abbas, M. Shafiee, "Structural health monitoring (SHM) and determination of surface defects in large metallic structures using ultrasonic guided waves," *Sensors (Switzerland)*, vol. 18, no. 11, 2018, 10.3390/s18113958.
[12] G.P.M. Fierro, D. Calla', D. Ginzburg, F. Ciampa, M. Meo, Nonlinear ultrasonic stimulated thermography for damage assessment in isotropic fatigued structures, J. Sound Vib. 404 (2017) 102–115.
[13] F. Ciampa, P. Mahmoodi, F. Pinto, M. Meo, Recent advances in active infrared thermography for non-destructive testing of aerospace components, Sensors (Switzerland). 18 (2) (2018) 609.
[14] M.P. De Goeje, K.E.D. Wapenaar, Non-destructive inspection of carbon fibre-reinforced plastics using eddy current methods, Composites 23 (3) (1992) 147–157.
[15] X.E. Gros, An eddy current approach to the detection of damage caused by low-energy impacts on carbon fibre reinforced materials, Mater. Des. 16 (3) (1995) 167–173.
[16] C. Bonavolonta, G. Peluso, G.P. Pepe, M. Valentino, Detection of early stage damage in carbon fiber reinforced polymers for aeronautical applications using an HTS SQUID magnetometer, Eur. Phys. J. B 42 (4) (2004) 491–496.
[17] K. Koyama, H. Hoshikawa, G. Kojima, "Eddy current nondestructive testing for carbon fiber-reinforced composites", *Journal of Pressure Vessel Technology*, Trans. ASME (2013), https://doi.org/10.1115/1.4023253.
[18] A. Katunin, Impact damage assessment in composite structures based on multiwavelet analysis of modal shapes, Indian J. Eng. Mater. Sci. (2015).
[19] G. F. Gomes, Y. A. D. Mendéz, P. da Silva Lopes Alexandrino, S. S. da Cunha, and A. C. Ancelotti, "The use of intelligent computational tools for damage detection and identification with an emphasis on composites – A review," *Composite Structures*, vol. 196, no. September 2017, pp. 44–54, 2018, 10.1016/j.compstruct.2018.05.002.
[20] H. Hu, B.-T. Wang, C.-H. Lee, J.-S. Su, Damage detection of surface cracks in composite laminates using modal analysis and strain energy method, Compos. Struct. 74 (4) (2006) 399–405.
[21] C.A. Geweth, F.S. Khosroshahi, K. Sepahvand, C. Kerkeling, S. Marburg, Damage Detection of Fibre-Reinforced Composite Structures Using Experimental Modal Analysis, Procedia Eng. 199 (2017) 1900–1905.
[22] C. Kralovec, M. Schagerl, Review of structural health monitoring methods regarding a multi-sensor approach for damage assessment of metal and composite structures, Sensors (Switzerland) 20 (3) (2020) 1–25, https://doi.org/10.3390/s20030826.
[23] R.N. Yancey, J.A. Smith, Non-destructive evaluation of advanced composites using high-resolution computed tomography, Natl. SAMPE Techn. Conference (1990).
[24] R.N. Yancey, G.Y. Baaklini, S.J. Klima, NDE of advanced turbine engine components and materials by computed tomography, in: In *ProceedIngs of the ASME Turbo Expo*, 1991, https://doi.org/10.1115/91-GT-287.
[25] S.C. Garcea, Y. Wang, P.J. Withers, X-ray computed tomography of polymer composites, Compos. Sci. Technol. 156 (2018) 305–319.
[26] P. Wagner, O. Schwarzhaupt, M. May, In-situ X-ray computed tomography of composites subjected to fatigue loading, Mater. Lett. 236 (2019) 128–130.
[27] A. Rashidi, T. Olfatbakhsh, B. Crawford, A.S. Milani, A review of current challenges and case study toward optimizing micro-computed X-ray tomography of carbon fabric composites, Materials. 13 (16) (2020) 3606.
[28] V. Giurgiutiu, Structural health monitoring with piezoelectric wafer active sensors, in: in *16th International Conference on Adaptive Structures and Technologies*, 2006, https://doi.org/10.1016/c2013-0-00155-7.
[29] S. Metaxa, K. Kalkanis, C.S. Psomopoulos, S.D. Kaminaris, G. Ioannidis, A review of structural health monitoring methods for composite materials, Procedia Struct. Integrity 22 (2019) (2019) 369–375, https://doi.org/10.1016/j.prostr.2020.01.046.
[30] A.J. Croxford, P.D. Wilcox, B.W. Drinkwater, G. Konstantinidis, Strategies for guided-wave structural health monitoring, Proc. R. Soc. A. 463 (2087) (2007) 2961–2981.
[31] A. De Luca, D. Perfetto, A. De Fenza, G. Petrone, F. Caputo, Guided wave SHM system for damage detection in complex composite structure, Theor. Appl. Fract. Mech. (2020), https://doi.org/10.1016/j.tafmec.2019.102408.
[32] T. Kundu, Acoustic source localization, Ultrasonics (2014), https://doi.org/10.1016/j.ultras.2013.06.009.
[33] H. Lamb, "On waves in an elastic plate," *Proceedings of the Royal Society of London. Series A, Containing Papers of a Mathematical and Physical Character*, 1917, 10.1098/rspa.1917.0008.
[34] M.R. Gorman, Plate wave acoustic emission, J. Acoust. Soc. Am. 90 (1) (1991) 358–364, https://doi.org/10.1121/1.401258.
[35] W.H. Prosser, M.R. Gorman, Plate mode velocities in graphite/epoxy plates, J. Acoust. Soc. Am. 96 (2) (1994) 902–907, https://doi.org/10.1121/1.410265.
[36] N. E. Huang *et al.*, "The empirical mode decomposition and the Hubert spectrum for nonlinear and non-stationary time series analysis," *Proceed. Roy. Soc. A: Mathemat., Phys. Eng. Sci.*, 1998, 10.1098/rspa.1998.0193.
[37] B. Yoo, D. Pines, and A. S. Purekar, "Guided lamb wave interrogation of a curved composite plate [0/90] using the Hilbert-Huang transform approach," in *Proceedings of the ASME Conference on Smart Materials, Adaptive Structures and Intelligent Systems, SMASIS2008*, 2008. 10.1115/SMASIS2008-591.
[38] G. Siracusano, et al., A framework for the damage evaluation of acoustic emission signals through Hilbert-Huang transform, Mech. Syst. Sig. Process. (2016), https://doi.org/10.1016/j.ymssp.2015.12.004.
[39] Y. Zhang, S. Wang, S. Huang, W. Zhao, Mode Recognition of Lamb Wave Detecting Signals in Metal Plate Using the Hilbert-Huang Transform Method, J Sens Technol (2015), https://doi.org/10.4236/jst.2015.51002.
[40] S. Pavlopoulou, W.J. Staszewski, C. Soutis, Evaluation of instantaneous characteristics of guided ultrasonic waves for structural quality and health monitoring, Struct. Control Health Monit. (2013), https://doi.org/10.1002/stc.1506.
[41] I. Das, M.T. Arif, A.M.T. Oo, M. Subhani, An improved hilbert-huang transform for vibration-based damage detection of utility timber poles, Appl. Sci. (Switzerland) (2021), https://doi.org/10.3390/app11072974.
[42] Z.K. Peng, P.W. Tse, F.L. Chu, An improved Hilbert-Huang transform and its application in vibration signal analysis, J. Sound Vib. (2005), https://doi.org/10.1016/j.jsv.2004.10.005.

[43] L. Cohen, *Time Frequancy Analysis*. 1995.
[44] F. Hlawatsch and F. Auger, *Time-Frequency Analysis: Concepts and Methods*. 2010. 10.1002/9780470611203.
[45] Y. Meyer, Wavelet. Operat. (1993), https://doi.org/10.1017/cbo9780511623820.
[46] A. Graps, An Introduction to Wavelets, IEEE Comput. Sci. Eng. 2 (2) (1995) 50–61, https://doi.org/10.1109/99.388960.
[47] K. Gröchenig, Foundations of time-frequency analysis, Appl. Math. (2003), https://doi.org/10.5860/choice.39-2814.
[48] M.B. Priestley, Evolutionary Spectra and Non-Stationary Processes, J. R. Stat. Soc. 27 (2) (1965) 204–237.
[49] M.A. Merrifield, R.T. Guza, Detecting Propagating Signals with Complex Empirical Orthogonal Functions: A Cautionary Note, J. Phys. Oceanogr. (1990), https://doi.org/10.1175/1520-0485(1990)020<1628:dpswce>2.0.co;2.
[50] N.E. Huang, S.S.P. Shen, Hilbert-huang transform and its applications. (2005), https://doi.org/10.1142/5862.
[51] N.E. Huang, Z. Shen, S.R. Long, A new view of nonlinear water waves: The Hilbert spectrum, Annu. Rev. Fluid Mech. (1999), https://doi.org/10.1146/annurev.fluid.31.1.417.
[52] W. H. Prosser, M. R. Gorman, and D. H. Humes, "Acoustic Emission Signals in Thin Plates Produced by Impact Damage," J. Acoust. Emiss., vol. 17(1–2), no. June 1998, pp. 29–36, 1999.
[53] Y. Mizutani, K. Nagashima, M. Takemoto, K. Ono, Fracture mechanism characterization of cross-ply carbon-fiber composites using acoustic emission analysis, NDT and E Int. (2000), https://doi.org/10.1016/S0963-8695(99)00030-4.
[54] H. Suzuki, T. Kinjo, Y. Hayashi, M. Takemoto, K. Ono, Wavelet transform of acoustic emission signals, J. Acoust. Emiss. (1996).
[55] Q.H.K. Ono, Pattern recognition analysis of acoustic emission signals, NDT and E Int. (1997), https://doi.org/10.1016/s0963-8695(97)85517-x.
[56] D. Guo, A. Mal, K. Ono, Wave theory of acoustic emission in composite laminates, J. Acoust. Emission (1996).
[57] M. Bourchak, I.R. Farrow, I.P. Bond, C.W. Rowland, F. Menan, Acoustic emission energy as a fatigue damage parameter for CFRP composites, Int. J. Fatigue (2007), https://doi.org/10.1016/j.ijfatigue.2006.05.009.
[58] M. Eaton, M. May, C. Featherston, K. Holford, S. Hallet, R. Pullin, Characterisation of damage in composite structures using acoustic emission, J. Phys. Conf. Ser. (2011), https://doi.org/10.1088/1742-6596/305/1/012086.
[59] A. Gupta, J.C. Duke, Identifying the arrival of extensional and flexural wave modes using wavelet decomposition of ultrasonic signals, Ultrasonics (2018), https://doi.org/10.1016/j.ultras.2017.09.008.
[60] R. James, R.P. Joseph, V. Giurgiutiu, Impact damage ascertainment in composite plates using in-situ acoustic emission signal signature identification, J. Compos. Sci. (2021), https://doi.org/10.3390/jcs5030079.
[61] M. Saeedifar, D. Zarouchas, Damage characterization of laminated composites using acoustic emission: A review, Compos. B Eng. (2020), https://doi.org/10.1016/j.compositesb.2020.108039.
[62] R. El Guerjouma, et al., Non-destructive evaluation of damage and failure of fibre reinforced polymer composites using ultrasonic waves and acoustic emission, Adv. Eng. Mater. (2001), https://doi.org/10.1002/1527-2648(200108)3:8<601::AID-ADEM601>3.0.CO;2-9.
[63] Z. Su, L. Ye, "Identification of Damage Using Lamb Waves: From Fundamentals to Applications," Lect. Notes Appl. Computat. Mechan., 2009, 10.1007/ 978-1-84882-784-4.
[64] C. Ramadas, K. Balasubramaniam, M. Joshi, C.V. Krishnamurthy, Interaction of the primary anti-symmetric Lamb mode (Ao) with symmetric delaminations: Numerical and experimental studies, Smart Mater. Struct. (2009), https://doi.org/10.1088/0964-1726/18/8/085011.
[65] U.K. Vaidya, Impact response of laminated and sandwich composites, CISM International Centre for Mechanical Sciences, Courses and Lectures 526 (2011) 97–191, https://doi.org/10.1007/978-3-7091-0523-8_4.
[66] S. Abrate, The Dynamics of Impact on Composite Structures, Key Eng. Mater. 141–143 (1998) 671–694, https://doi.org/10.4028/www.scientific.net/KEM.141-143.671.
[67] ASTM International, ASTM D7136 / D7136M–15, Standard Test Method for Measuring the Damage Resistance of a Fiber-Reinforced Polymer Matrix Composite to a Drop-Weight Impact Event, ASTM Book of Standards Volume (2015).
[68] P. Gaudenzi, M. Bernabei, E. Dati, G. de Angelis, M. Marrone, L. Lampani, On the evaluation of impact damage on composite materials by comparing different NDI techniques, Compos. Struct. (2014), https://doi.org/10.1016/j.compstruct.2014.07.048.
[69] E. Giannaros, et al., Low- and high-fidelity modeling of sandwich-structured composite response to bird strike, as tools for a digital-twin-assisted damage diagnosis, Int. J. Impact Eng (2022), https://doi.org/10.1016/j.ijimpeng.2021.104058.